

Optimizing surface defects for atomic-scale electronics: Si dangling bonds

Peter Scherpelz^{1,*} and Giulia Galli^{1,2}

¹*Institute for Molecular Engineering, The University of Chicago, Chicago, IL, USA*

²*Materials Science Division, Argonne National Laboratory, Argonne, IL, USA*

(Dated: October 12, 2018)

Surface defects created and probed with scanning tunneling microscopes are a promising platform for atomic-scale electronics and quantum information technology applications. Using first-principles calculations we demonstrate how to engineer dangling bond (DB) defects on hydrogenated Si(100) surfaces, which give rise to isolated impurity states that can be used in atomic-scale devices. In particular we show that sample thickness and biaxial strain can serve as control parameters to design the electronic properties of DB defects. While in thick Si samples the neutral DB state is resonant with bulk valence bands, ultrathin samples (1–2 nm) lead to an isolated impurity state in the gap; similar behavior is seen for DB pairs and DB wires. Strain further isolates the DB from the valence band, with the response to strain heavily dependent on sample thickness. These findings suggest new methods for tuning the properties of defects on surfaces for electronic and quantum information applications. Finally, we present a consistent and unifying interpretation of many results presented in the literature for DB defects on hydrogenated silicon surfaces, rationalizing apparent discrepancies between different experiments and simulations.

The ability to engineer semiconducting devices at the atomic scale is key to achieving further miniaturization of electronics, and to using the quantum nature of point defects for quantum information applications. One promising atomic-scale fabrication method employs scanning tunneling microscopy (STM) to create and manipulate defects on semiconducting surfaces [1]. For example, dangling bonds (DBs) have been created and successfully manipulated on hydrogen-terminated Si(100) surfaces by desorbing individual H atoms from the substrate [2]. Ensembles of DBs on silicon surfaces are now widely used to create atomically-precise systems of defects [3–15], leveraging expertise with the fabrication of silicon devices, including the ability to produce clean and regular hydrogen-terminated surfaces.

Numerous experiments have demonstrated many attractive properties and potential applications of DBs on H:Si(100). These defects interact over next-nearest neighbor distances [3, 4, 6], and the charge of individual DBs can be reversibly manipulated, with given charge states persisting for hours [5]. In addition, these DBs display negative differential resistance, potentially providing a new component for atomic-scale electronic circuitry [12]. Theoretical work has suggested that pairs of DBs may be used to create a charge qubit [16]. Furthermore, DBs may be assembled into specific patterns for electronics or quantum simulations [6, 14, 17, 18], including one-dimensional conducting or semiconducting wires [7, 19, 20]. They further serve as a starting configuration for atomically-precise dopant placement [21–25]. Hence tuning and manipulating the properties of DBs, e.g., charge states, may lead to a promising strategy to build a flexible atomic-scale platform of defects for electronic and quantum information technology applications.

In this work, using the results of first-principles calculations we propose ways to realize DB defect states on

H:Si(100) with energies within the electronic gap of bulk Si; in particular we show how to tune sample thickness and strain to obtain desired energy and charge states. While doing so, we also address existing controversies present in the literature on the properties of DB states on Si surfaces. We present a consistent interpretation of previous results, and use advanced methods to ensure our findings are robust. We first show how the thickness of the Si sample can be manipulated to alter the electronic properties of the neutral Si DB state, and we demonstrate that a stable positively-charged DB state is accessible only in thin (1.2 nm) Si samples. We also present similar effects for multiple DB systems. We then turn our attention to the effect of biaxial strain, showing that the electronic response of defects to strain depends significantly on the slab thickness. We propose that by combining thickness and strain, one may engineer the properties of neutral DB defects for use in atomic-scale electronics.

Methods: We carried out density functional theory (DFT) [26, 27] calculations with plane-wave basis sets and norm-conserving pseudopotentials [28, 29] using the QUANTUM ESPRESSO package [30, 31]. We modeled Si DBs on an H-terminated Si(100) slab periodically repeated in two directions and having a finite number of layers in the third, with vacuum separating periodic images. All neutral DB calculations were spin-polarized. Atomic geometries were optimized until forces on the atoms were less than 0.013 eV/Å.

We used the gradient-corrected exchange-correlation functional developed by Perdew, Burke, and Ernzerhof (PBE) [32], as well as hybrid functionals [33]. In particular we adopted a dielectric-dependent hybrid with the fraction of exact exchange $\alpha = 0.085 \approx 1/\epsilon_{\infty}^{\text{Si}}$, shown to reproduce accurately the electronic properties of bulk Si [34]. We also used the Heyd-Scuseria-Ernzerhof (HSE)

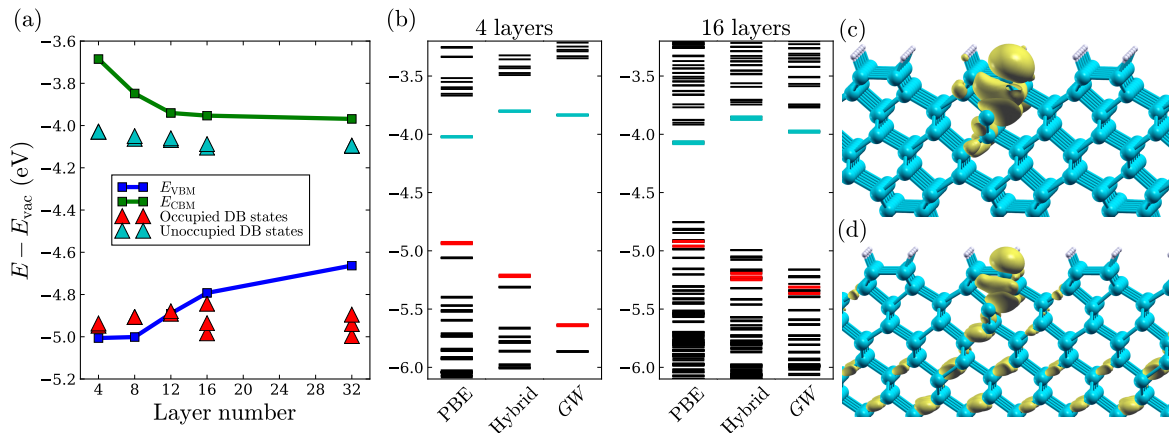


FIG. 1. Electronic properties of neutrally charged dangling bonds on an H-terminated Si(100) slab. (a) Variation of the valence band maximum (VBM), conduction band minimum (CBM), and dangling bond (DB) energy levels with layer number included in a model Si slab, as obtained using density functional theory (DFT) calculations at the PBE level. We estimate that for slab thicknesses of 8 nm or greater, the DB position is about 0.3 eV below the VBM. (b) Energy levels at the Γ point of the slab Brillouin zone, as obtained with DFT using gradient-corrected (PBE) and dielectric-dependent hybrid functionals, and many-body perturbation theory calculations (*GW*). Results for 4- and 16-layer slabs are displayed. As in (a), red (cyan) designates energy levels of occupied (unoccupied) DB states. (c) Isosurface of the wavefunction amplitude for an isolated DB state in an H-terminated 8-layer Si slab. (d) Isosurface of the wavefunction amplitude for a DB state hybridized with a bulk state in an H-terminated 16-layer Si slab. See SM for details.

functional [35, 36] to compare with previous work. In addition, for selected configurations we performed many-body perturbation theory (MBPT) calculations [37–39] at the G_0W_0 level using the WEST software package [40–42]. Within G_0W_0 the exchange-correlation energy entering DFT is replaced by an electronic self-energy calculated using the screened Coulomb interaction and the Green’s function. WEST uses spectral decomposition techniques [40, 43–46] and methods based on density functional perturbation theory [47] to optimize calculations for large systems [40].

Details of geometries, calculation parameters, convergence tests, and identification of DB states, can be found in the Supplemental Material (SM).

Results: Multiple computational results have been reported in the literature for the singly-occupied, neutral DB (DB^0) state, relative to the VBM of Si: -0.3 eV [48], 0.013 eV [6], 0.2 eV [49], 0.35 eV [16, 50], 0.36 eV [7], and 0.42 eV [51] (other calculations [5, 11, 52] only addressed doped systems and/or charged DBs) [53]. These results differ quantitatively and qualitatively: indeed, a defect state located in energy above the VBM is expected to be well-isolated electronically, whereas one below may instead hybridize with other electronic states in the material and hence may not be amenable to manipulation.

In order to rationalize the various literature values for the DB^0 , we calculated its electronic properties for many model slabs, differing by the number of layers and supercell lattice constant. We found that the choice of lattice constants in the plane perpendicular to the surface primarily influenced the degree of dispersion of the DB state

(see SM for details). We observed instead a much more pronounced dependence of the nature of the DB state on the thickness of the slab, as shown in Figure 1(a). Its energy relative to the vacuum energy of the supercell model is roughly constant. However, the positions of the VBM and conduction band minimum (CBM) vary significantly with the number of layers in the slab. In general quantum confinement leads to a larger bandgap whose convergence toward the bulk value is very slow as a function of the slab layer number [54, 55]. A similar dependence on thickness was recently found for a bare Si(100)- $p(2\times 2)$ surface [56].

Figure 1(a) shows that for a slab 8 layers thick (≈ 1.2 nm) the DB energy is 0.09 eV above the VBM energy, while for a 16-layer slab (≈ 2.3 nm) its energy is 0.05 eV to 0.19 eV below the VBM energy. The DB^0 state is well-isolated for 8 or fewer layer slabs, while it is mixed with bulk Si states for 16 or more layers, as shown in Figure 1(c-d). To verify these findings are robust with respect to the level of theory used, we carried out additional calculations using dielectric-dependent hybrid functionals and MBPT. Figure 1(b) shows that the position of the occupied DB state relative to the VBM is nearly the same at all levels of theory. Hybrid and *GW* calculations significantly correct the bandgap energy found at the PBE level, but leave the DB state positions relative to the VBM and CBM unchanged.

Hence we conclude that for Si samples 1.2 nm or thinner, the neutral singly-occupied DB state falls within the bulk gap, while for samples 2.3 nm or thicker, it is hybridized with bulk states and resides below the VBM.

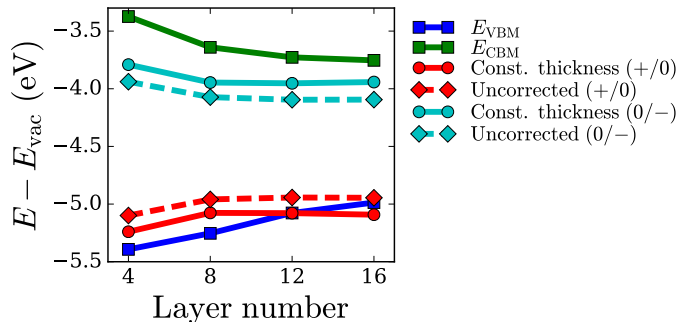


FIG. 2. Calculated adiabatic charge transition levels of a DB on an H-terminated Si(100) surface, as a function of the sample thickness, using the dielectric-dependent hybrid functional. E_{VBM} and E_{CBM} indicate the energies of the valence band minimum and the conduction band maximum, respectively. Uncorrected results omit the finite size scaling corrections obtained with the method of Ref. [52].

We expect the DB^0 state to have a much shorter coherence time for thickness > 2.3 nm, impacting its behavior in quantum information applications. However, in other applications, its hybridization with bulk states of thick slabs may be beneficial by facilitating long-range interactions between point defects.

We note that these DB properties are different from those of Si DBs at a Si/SiO₂ interface, for which the energy of the neutral defect is found by electron paramagnetic resonance to reside in the gap of bulk Si [57]. This difference is presumably due to the significantly different environment surrounding DBs in the two systems [51]. We also stress that the behavior above is not due to a change in the net magnetization density (which is not significant as a function of layer thickness), but rather is due to changes in the energy level of the singly-occupied DB, which is an isolated defect state for thin slabs but a resonant defect state for thick slabs.

While understanding the properties of the neutral DB is important for potential quantum information applications, charge transition energy levels (CTLs) are the quantities of interest for scanning tunneling spectroscopy observations [5, 7–12], and applications for electronics [5, 12] or charge qubits [16]. We obtained CTLs by computing total energies of different charge states in their respective optimized geometries (thus calculating adiabatic transitions), taking into account corrections for the Coulomb interaction of periodic images, and alignment of the electrostatic potential between configurations [58]. For surfaces, correction methods used in bulk systems are not applicable due to the large variation in dielectric constant between the bulk and vacuum. We followed the prescription suggested in Ref. [52]. Briefly, a sawtooth electric field is used to compute the z -dependent dielectric constant, from which a periodic electrostatic model of the charged defect is constructed. The electrostatic energy is then calculated using finite size scaling by ex-

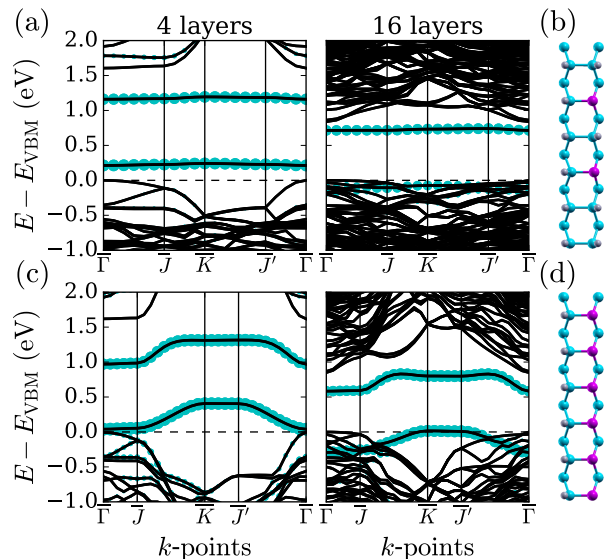


FIG. 3. Electronic properties of multiple-DB systems. (a) Band structure of a neutral DB pair. (b) Model of the DB pair system. Si DBs are highlighted. (c) Band structure of the anti-ferromagnetic DB wire. Cyan circles in (a) and (c) show the overlap of states with the Si atoms containing the DBs. (d) Model of the DB wire. Si DBs are highlighted. The neutral, singly-occupied DBs have alternating spin-up and spin-down configurations.

trapolating the energy of the model computed for cells of increasing sizes. As we were interested specifically in the properties of thin Si slabs, we kept the slab height constant during extrapolation.

Calculations at the PBE level of theory were performed to check for convergence, and consistent results were found, within ± 0.1 eV, when varying vacuum length of the supercell by a factor of 2 and horizontal supercell area by a factor of 2.7. Figure 2 shows our results using the dielectric-dependent hybrid functional. Qualitatively, the PBE results are similar to those in Figure 2, with a 0.2 eV decrease in the (+/0) CTL relative to the VBM (see SM).

Figure 2 shows that for thick samples (> 2.3 nm), only the (0/−) CTL falls within the bulk Si bandgap. This result is consistent with the experimental observation showing long lifetimes of both the DB^0 and DB^- charge states, when the DB is appropriately charged by an STM tip which is then removed [5]. No long-lived DB^+ state was detected experimentally, even though a p -type Si sample was used [5]. Interestingly, Figure 2 also shows that very thin samples may exhibit long-lived DB^+ states without requiring any other perturbations, making all three charge states easily accessible. Such a system may provide a flexible platform for quantum information technology applications.

Arrangements of multiple DBs lead to additional possibilities for atomic-scale electronics. We considered two

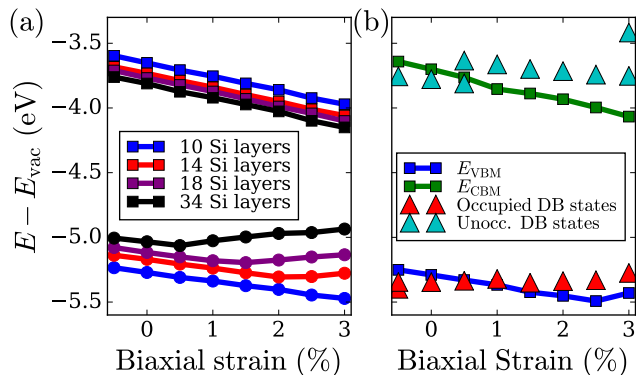


FIG. 4. Variation of electronic properties as a function of biaxial strain applied to the Si slab. (a) Variation of the valence band maximum (VBM, circles) and conduction band minimum (CBM, squares) positions vs. strain. For all values of strain, the bandgap for 34-layer slabs is within 0.1 eV of the bulk bandgap. (b) Variation of VBM and CBM positions, and the energies of DB states, for a 10-layer system.

prototypical multiple-DB systems, and we found that they exhibit the same properties as a single DB, as a function of thickness. Figure 3(a) shows the band structure of a neutral DB pair [4, 6, 16]. Its geometry (Figure 3(b)) is an example of that proposed for charge qubits [4, 16]. For a 4-layer slab all DB states are well-separated, while for a 16-layer slab the occupied DB states become resonant with the valence band. The presence of this resonance may lead to stronger interactions between bulk and DB states; the overall larger gap for a 4-layer system should also improve addressability of the DB pair using mid-infrared lasers [59].

Figure 3(c) shows the band structure of the anti-ferromagnetic DB wire in Figure 3(d) [7, 19, 20, 60–64]. For a neutral DB wire on a 4-layer slab, both the occupied and unoccupied one-dimensional (1D) bands lie within the gap, and thus the wire may conduct either electron or hole states under suitable bias. In contrast, for a 16-layer slab, only the unoccupied 1D band lies within the gap, while the occupied 1D band is resonant with the bulk Si states. Thus, for 16 layers, hole conduction would be expected to occur through both bulk and wire states when a suitable bias is applied, removing the 1D nature of the conductivity.

A recent theoretical study raised the intriguing possibility of using strain to isolate surface states of a bare Si(100) surface, showing that the VBM is lowered in energy when biaxial tensile strain is applied in the horizontal directions [65]. However, this result is not consistent with those of theoretical and experimental investigations of bulk Si under biaxial tensile strain, showing that the VBM energy increases and the bulk bandgap decreases [66, 67]. Our results indicate that for standard (thick) silicon surfaces, strain will not isolate surface states, in contrast to the conclusions of Ref. [65]. Instead, only for

thin Si slabs can strain be used to isolate surface states, a result of the remarkably different response to strain for thin slabs compared to bulk systems. Figure 4(a) shows this difference in response: the VBM position as a function of strain shows a qualitatively different trend for thick ($\gtrsim 4$ nm) slabs, where it increases with strain, and thin (10-layer, 1.5 nm) slabs, where it decreases with strain to a thickness-dependent minimum. As a result, for thick slabs the fundamental gap remains close to that of the bulk, but for thin slabs tensile strain leads to an increase of the gap relative to that of the bulk. An unstrained 10-layer slab has a fundamental gap 0.4 eV larger than that of bulk Si. In contrast, under 3% biaxial tensile strain its fundamental gap is 0.8 eV larger than that of the bulk.

Thus, while in thick slabs biaxial tensile strain would not be expected to aid in isolating DB states, in very thin slabs, the opposite is true, as shown in Figure 4(b). A state which is not well-isolated in a 1.5 nm unstrained slab becomes isolated for strains of 1% or more. For direct comparison with Ref. [65], results in Figure 4 used the HSE hybrid functional; calculations with PBE showed the same trend as a function of strain (see SM). Note that Ref. [65] used a 10-layer slab model, effectively reporting results applicable only to thin slabs.

In summary, we have proposed how to engineer the properties of DBs on hydrogenated Si surfaces by varying sample thickness and applied stress. We have shown that the single particle energy and wavefunction of DBs on H:Si(100)-(2 \times 1) may be more readily isolated from those of bulk states in thin samples (< 1.2 nm) than in bulk-like slabs. Specifically, in thin samples, the neutral DB state is well above the VBM, and three charge states may be stabilized. In thick (> 2.3 nm) samples, the neutral DB state is instead hybridized with bulk states, and the positively charged DB is not stable; for bulk samples the neutral DB state is about 0.3 eV below the VBM. We verified that our results are robust with respect to the level of first-principles theory used, including semi-local and hybrid functionals and many-body perturbation theory.

Dangling bond pairs and wires showed the same response to sample thickness. Notably, thin samples allow hole conduction along isolated DB wires, whereas in thick samples conduction would also occur through the bulk. Additionally, we found that in thin samples biaxial tensile strain will further isolate the DB energy from that of the VBM. However, strain is not helpful in isolating states in thick Si samples.

We emphasize the importance of carrying out accurate calculations, numerically converged and at a high level of theory, in order to determine the properties of isolated DBs. Although numerous experimental STM studies have been performed, both tip-induced band bending and non-equilibrium charging did not allow for a clear extrapolation of results to isolated DB configurations [5–

12]. Furthermore, recent work has shown that nearby dopants can affect the behavior of DBs [10], which further complicates the interpretation of experimental findings. Our study of electronic properties as a function of film thickness was able to reconcile apparent discrepancies found in published results, which were reported for different numbers of layers in the slabs and sometimes interpreted as representative of bulk samples (we estimate that 60 layers are necessary for calculations to be representative of thick, bulk-like samples).

A question remains on the experimental realization of the thin films proposed here as promising platforms. Si films as thin as 3 nm have been reported [68]; strained Si-on-insulator samples less than 10 nm thick have also been fabricated [69]. While the 1-2 nm slabs considered here may require new techniques, their experimental realization appears possible in the near future. Finally, we expect the results found here for DBs may be valid for several other defects when placed in thin Si slabs. This includes many defects used in quantum information applications, such as isolated phosphorous [70, 71], boron [72], bismuth [73, 74], or selenium [75, 76] dopants, as well as patterned surface systems [6, 14, 17, 18]. Indeed the electronic properties of the DBs change as a function of thickness due to the change of the VBM and CBM themselves, not because of a substantial shift of the defect level. Hence the combination of strain and thickness proposed here to isolate DB defects and stabilize multiple charge states should be generalizable to other types of defects.

We gratefully acknowledge Hosung Seo, Marco Govoni, David Schuster, Jeff Guest, Pamela Peña Martin, John Randall, James Owen, Scott Schmucker, Neil Curson and Hannu-Pekka Komsa for helpful conversations. This research was supported by an appointment (P.S.) to the Intelligence Community Postdoctoral Research Fellowship Program at The University of Chicago, administered by Oak Ridge Institute for Science and Education through an interagency agreement between the U.S. Department of Energy and the Office of the Director of National Intelligence. This work (G.G.) was also supported by MICCoM as part of the Computational Materials Sciences Program funded by the U.S. Department of Energy, Office of Science, Basic Energy Sciences, Materials Sciences and Engineering Division through Argonne National Laboratory, under contract number DE-AC02-06CH11357. An award of computer time was provided by the Innovative and Novel Computational Impact on Theory and Experiment (INCITE) program. This research used resources of the Argonne Leadership Computing Facility, which is a DOE Office of Science User Facility supported under Contract DE-AC02-06CH11357 (*GW* calculations), resources of the National Energy Research Scientific Computing Center, a DOE Office of Science User Facility supported by the Office of Science of the U.S. Department of Energy under Contract No. DE-

AC02-05CH11231 (hybrid calculations), and resources provided by the University of Chicago Research Computing Center.

* pscherpelz@uchicago.edu

- [1] Floris A. Zwanenburg, Andrew S. Dzurak, Andrea Morello, Michelle Y. Simmons, Lloyd C. L. Hollenberg, Gerhard Klimeck, Sven Rogge, Susan N. Coppersmith, and Mark A. Eriksson, “Silicon quantum electronics,” *Rev. Mod. Phys.* **85**, 961–1019 (2013).
- [2] J. W. Lyding, T.-C. Shen, J. S. Hubacek, J. R. Tucker, and G. C. Abeln, “Nanoscale patterning and oxidation of H-passivated Si(100)-2x1 surfaces with an ultrahigh vacuum scanning tunneling microscope,” *Appl. Phys. Lett.* **64**, 2010–2012 (1994).
- [3] M. Baseer Haider, Jason L. Pitters, Gino A. DiLabio, Lucian Livadaru, Josh Y. Mutus, and Robert A. Wolkow, “Controlled coupling and occupation of silicon atomic quantum dots at room temperature,” *Phys. Rev. Lett.* **102**, 046805 (2009).
- [4] Jason L. Pitters, Lucian Livadaru, M. Baseer Haider, and Robert A. Wolkow, “Tunnel coupled dangling bond structures on hydrogen terminated silicon surfaces,” *J. Chem. Phys.* **134**, 064712 (2011).
- [5] Amandine Bellec, Laurent Chaput, Gérald Dujardin, Damien Riedel, Louise Stauffer, and Philippe Sonnet, “Reversible charge storage in a single silicon atom,” *Phys. Rev. B* **88**, 241406 (2013).
- [6] S. R. Schofield, P. Studer, C. F. Hirjibehedin, N. J. Curson, G. Aeppli, and D. R. Bowler, “Quantum engineering at the silicon surface using dangling bonds,” *Nat. Commun.* **4**, 1649 (2013).
- [7] Wei Ye, Kyoungmin Min, Pamela Peña Martin, Angus A. Rockett, N. R. Aluru, and Joseph W. Lyding, “Scanning tunneling spectroscopy and density functional calculation of silicon dangling bonds on the Si(100)-2x1:H surface,” *Surf. Sci.* **609**, 147–151 (2013).
- [8] Marco Taucer, Lucian Livadaru, Paul G. Piva, Roshan Achal, Hatem Labidi, Jason L. Pitters, and Robert A. Wolkow, “Single-electron dynamics of an atomic silicon quantum dot on the H-Si(100)-(2x1) surface,” *Phys. Rev. Lett.* **112**, 256801 (2014).
- [9] Marek Kolmer, Szymon Godlewski, Rafal Zuzak, Mateusz Wojtaszek, Caroline Rauer, Aurélie Thuaiere, Jean-Michel Hartmann, Hubert Moriceau, Christian Joachim, and Marek Szymonski, “Atomic scale fabrication of dangling bond structures on hydrogen passivated Si(001) wafers processed and nanopackaged in a clean room environment,” *Appl. Surf. Sci.* **288**, 83–89 (2014).
- [10] Hatem Labidi, Marco Taucer, Mohammad Rashidi, Mohammad Koleini, Lucian Livadaru, Jason Pitters, Martin Cloutier, Mark Salomons, and Robert A. Wolkow, “Scanning tunneling spectroscopy reveals a silicon dangling bond charge state transition,” *New J. Phys.* **17**, 073023 (2015).
- [11] Hiroyo Kawai, Olga Neucheva, Tiong Leh Yap, Christian Joachim, and Mark Saeys, “Electronic characterization of a single dangling bond on n- and p-type Si(001)-(2x1):H,” *Surf. Sci.* **645**, 88–92 (2016).
- [12] Mohammad Rashidi, Marco Taucer, Isil Ozfidan, Erika

- Lloyd, Mohammad Koleini, Hatem Labidi, Jason L. Pitters, Joseph Maciejko, and Robert A. Wolkow, “Time-resolved imaging of negative differential resistance on the atomic scale,” *Phys. Rev. Lett.* **117**, 276805 (2016).
- [13] Taro Hitosugi, T. Hashizume, S. Heike, Y. Wada, S. Watanabe, T. Hasegawa, and K. Kitazawa, “Scanning tunnelling spectroscopy of dangling-bond wires fabricated on the Si(100)-2×1-H surface,” *Appl. Phys. A* **66**, S695–S699 (1998).
- [14] Laetitia Soukiassian, Andrew J. Mayne, Marilena Carbone, and Gérald Dujardin, “Atomic wire fabrication by STM induced hydrogen desorption,” *Surf. Sci. Proceedings of the Ninth International Workshop on Desorption Induced by Electronic Transitions*, **528**, 121–126 (2003).
- [15] A. J. Mayne, D. Riedel, G. Comtet, and G. Dujardin, “Atomic-scale studies of hydrogenated semiconductor surfaces,” *Prog. Surf. Sci.* **81**, 1–51 (2006).
- [16] Lucian Livadaru, Peng Xue, Zahra Shaterzadeh-Yazdi, Gino A DiLabio, Josh Mutus, Jason L Pitters, Barry C Sanders, and Robert A Wolkow, “Dangling-bond charge qubit on a silicon surface,” *New J. Phys.* **12**, 083018 (2010).
- [17] F. Ample, I. Duchemin, M. Hliwa, and C. Joachim, “Single OR molecule and OR atomic circuit logic gates interconnected on a Si(100)H surface,” *J. Phys.: Condens. Matter* **23**, 125303 (2011).
- [18] Mikael Kepenekian, Roberto Robles, Riccardo Rurali, and Nicolás Lorente, “Spin transport in dangling-bond wires on doped H-passivated Si(100),” *Nanotechnology* **25**, 465703 (2014).
- [19] Taro Hitosugi, S. Heike, T. Onogi, T. Hashizume, S. Watanabe, Z.-Q. Li, K. Ohno, Y. Kawazoe, T. Hasegawa, and K. Kitazawa, “Jahn-teller distortion in dangling-bond linear chains fabricated on a hydrogen-terminated Si(100)-2 × 1 surface,” *Phys. Rev. Lett.* **82**, 4034–4037 (1999).
- [20] Borislav Naydenov and John J. Boland, “Engineering the electronic structure of surface dangling bond nanowires of different size and dimensionality,” *Nanotechnology* **24**, 275202 (2013).
- [21] S. R. Schofield, N. J. Curson, M. Y. Simmons, F. J. Ruef, T. Hallam, L. Oberbeck, and R. G. Clark, “Atomically precise placement of single dopants in Si,” *Phys. Rev. Lett.* **91**, 136104 (2003).
- [22] Frank J. Ruess, Lars Oberbeck, Michelle Y. Simmons, Kuan Eng J. Goh, Alex R. Hamilton, Toby Hallam, Steven R. Schofield, Neil J. Curson, and Robert G. Clark, “Toward atomic-scale device fabrication in silicon using scanning probe microscopy,” *Nano Lett.* **4**, 1969–1973 (2004).
- [23] Martin Fuechsle, Jill A. Miwa, Suddhasatta Mahapatra, Hoon Ryu, Sunhee Lee, Oliver Warschkow, Lloyd C. L. Hollenberg, Gerhard Klimeck, and Michelle Y. Simmons, “A single-atom transistor,” *Nat. Nano.* **7**, 242–246 (2012).
- [24] B. Weber, S. Mahapatra, H. Ryu, S. Lee, A. Fuhrer, T. C. G. Reusch, D. L. Thompson, W. C. T. Lee, G. Klimeck, L. C. L. Hollenberg, and M. Y. Simmons, “Ohm’s law survives to the atomic scale,” *Science* **335**, 64–67 (2012).
- [25] Gavin W. Morley, “Chapter 3: Towards spintronic quantum technologies with dopants in silicon,” in *Electron Paramagnetic Resonance*, Vol. 24 (Royal Society of Chemistry, 2014) pp. 62–76.
- [26] P. Hohenberg and W. Kohn, “Inhomogeneous electron gas,” *Phys. Rev.* **136**, B864–B871 (1964).
- [27] W. Kohn and L. J. Sham, “Self-consistent equations including exchange and correlation effects,” *Phys. Rev.* **140**, A1133–A1138 (1965).
- [28] N. Troullier and José Luís Martins, “Efficient pseudopotentials for plane-wave calculations,” *Phys. Rev. B* **43**, 1993–2006 (1991).
- [29] Davide Ceresoli, “Pseudopotentials,” <https://sites.google.com/site/dceresoli/pseudopotentials>, (accessed May 20, 2016).
- [30] Paolo Giannozzi, Stefano Baroni, Nicola Bonini, Matteo Calandra, Roberto Car, Carlo Cavazzoni, Davide Ceresoli, Guido L. Chiarotti, Matteo Cococcioni, Ismaila Dabo, Andrea Dal Corso, Stefano de Gironcoli, Stefano Fabris, Guido Fratesi, Ralph Gebauer, Uwe Gerstmann, Christos Gougoussis, Anton Kokalj, Michele Lazzeri, Layla Martin-Samos, Nicola Marzari, Francesco Mauri, Riccardo Mazzarello, Stefano Paolini, Alfredo Pasquarello, Lorenzo Paulatto, Carlo Sbraccia, Sandro Scandolo, Gabriele Sciuozza, Ari P. Seitsonen, Alexander Smogunov, Paolo Umari, and Renata M. Wentzcovitch, “QUANTUM ESPRESSO: a modular and open-source software project for quantum simulations of materials,” *J. Phys.: Condens. Matter* **21**, 395502 (2009).
- [31] “QUANTUM ESPRESSO,” <http://www.quantum-espresso.org>, (accessed Jan 26, 2016).
- [32] John P. Perdew, Kieron Burke, and Matthias Ernzerhof, “Generalized gradient approximation made simple,” *Phys. Rev. Lett.* **77**, 3865–3868 (1996).
- [33] Stephan Kümmel and Leon Kronik, “Orbital-dependent density functionals: Theory and applications,” *Rev. Mod. Phys.* **80**, 3–60 (2008).
- [34] Jonathan H. Skone, Marco Govoni, and Giulia Galli, “Self-consistent hybrid functional for condensed systems,” *Phys. Rev. B* **89**, 195112 (2014).
- [35] Jochen Heyd, Gustavo E. Scuseria, and Matthias Ernzerhof, “Hybrid functionals based on a screened Coulomb potential,” *J. Chem. Phys.* **118**, 8207–8215 (2003).
- [36] Jochen Heyd, Gustavo E. Scuseria, and Matthias Ernzerhof, “Erratum: “Hybrid functionals based on a screened Coulomb potential” [J. Chem. Phys. 118, 8207 (2003)],” *J. Chem. Phys.* **124**, 219906 (2006).
- [37] Lars Hedin, “New method for calculating the one-particle Green’s function with application to the electron-gas problem,” *Phys. Rev.* **139**, A796–A823 (1965).
- [38] Mark S. Hybertsen and Steven G. Louie, “Electron correlation in semiconductors and insulators: Band gaps and quasiparticle energies,” *Phys. Rev. B* **34**, 5390–5413 (1986).
- [39] F. Aryasetiawan and O. Gunnarsson, “The GW method,” *Rep. Prog. Phys.* **61**, 237 (1998).
- [40] Marco Govoni and Giulia Galli, “Large scale GW calculations,” *J. Chem. Theory Comput.* **11**, 2680–2696 (2015).
- [41] Peter Scherpelz, Marco Govoni, Ikutaro Hamada, and Giulia Galli, “Implementation and validation of fully relativistic GW calculations: Spin-orbit coupling in molecules, nanocrystals, and solids,” *J. Chem. Theory Comput.* **12**, 3523–3544 (2016).
- [42] “WEST,” <http://www.west-code.org>, (accessed Jan 26, 2016).
- [43] Hugh F. Wilson, François Gygi, and Giulia Galli, “Efficient iterative method for calculations of dielectric matrices,” *Phys. Rev. B* **78**, 113303 (2008).
- [44] Hugh F. Wilson, Deyu Lu, François Gygi, and Giulia

- Galli, “Iterative calculations of dielectric eigenvalue spectra,” *Phys. Rev. B* **79**, 245106 (2009).
- [45] Huy-Viet Nguyen, T. Anh Pham, Dario Rocca, and Giulia Galli, “Improving accuracy and efficiency of calculations of photoemission spectra within the many-body perturbation theory,” *Phys. Rev. B* **85**, 081101 (2012).
- [46] T. Anh Pham, Huy-Viet Nguyen, Dario Rocca, and Giulia Galli, “*GW* calculations using the spectral decomposition of the dielectric matrix: Verification, validation, and comparison of methods,” *Phys. Rev. B* **87**, 155148 (2013).
- [47] Stefano Baroni, Stefano de Gironcoli, Andrea Dal Corso, and Paolo Giannozzi, “Phonons and related crystal properties from density-functional perturbation theory,” *Rev. Mod. Phys.* **73**, 515–562 (2001).
- [48] Jürgen Wierferink, Peter Krüger, and Johannes Pollmann, “Ab initio study of atomic hydrogen diffusion on the clean and hydrogen-terminated Si(001) surface,” *Phys. Rev. B* **82**, 075323 (2010).
- [49] Torbjörn Blomquist and George Kirczenow, “Controlling the charge of a specific surface atom by the addition of a non-site-specific single impurity in a Si nanocrystal,” *Nano Lett.* **6**, 61–65 (2006).
- [50] M. Baseer Haider, Jason L. Pitters, Gino A. DiLabio, Lucian Livadaru, Josh Y. Mutus, and Robert A. Wolkow, “Controlled coupling and occupation of silicon atomic quantum dots,” (2008), arXiv:0807.0609 [cond-mat].
- [51] Hassan Raza, “Theoretical study of isolated dangling bonds, dangling bond wires, and dangling bond clusters on a H:Si(001)-2x1 surface,” *Phys. Rev. B* **76**, 045308 (2007).
- [52] Hannu-Pekka Komsa and Alfredo Pasquarello, “Finite-size supercell correction for charged defects at surfaces and interfaces,” *Phys. Rev. Lett.* **110**, 095505 (2013).
- [53] Only the lowest two values from Refs. [6, 48] are explicitly spin-polarized; the calculations that cluster at 0.35-0.42 eV are thus unlikely to be physically accurate.
- [54] Yan Li and Giulia Galli, “Electronic and spectroscopic properties of the hydrogen-terminated Si(111) surface from ab initio calculations,” *Phys. Rev. B* **82**, 045321 (2010).
- [55] Massimo V. Fischetti, Bo Fu, Sudarshan Narayanan, and Jiseok Kim, “Semiclassical and quantum electronic transport in nanometer-scale structures: Empirical pseudopotential band structure, Monte Carlo simulations and Pauli master equation,” in *Nano-Electronic Devices*, edited by Dragica Vasileska and Stephen M. Goodnick (Springer New York, 2011) pp. 183–247.
- [56] Keisuke Sagisaka, Jun Nara, and David Bowler, “Importance of bulk states for the electronic structure of semiconductor surfaces: implications for finite slabs,” *J. Phys.: Condens. Matter* (2017), 10.1088/1361-648X/aa5f91.
- [57] P. M. Lenahan and J. F. Conley Jr., “What can electron paramagnetic resonance tell us about the Si/SiO₂ system?” *J. Vac. Sci. Technol. B* **16**, 2134 (1998).
- [58] Christoph Freysoldt, Blazej Grabowski, Tilmann Hickel, Jörg Neugebauer, Georg Kresse, Anderson Janotti, and Chris G. Van de Walle, “First-principles calculations for point defects in solids,” *Rev. Mod. Phys.* **86**, 253–305 (2014).
- [59] Zahra Shaterzadeh-Yazdi, Lucian Livadaru, Marco Taucer, Josh Mutus, Jason Pitters, Robert A. Wolkow, and Barry C. Sanders, “Characterizing the rate and coherence of single-electron tunneling between two dangling bonds on the surface of silicon,” *Phys. Rev. B* **89**, 035315 (2014).
- [60] Ji Young Lee, Jin-Ho Choi, and Jun-Hyung Cho, “Antiferromagnetic coupling between two adjacent dangling bonds on si(001): Total-energy and force calculations,” *Phys. Rev. B* **78**, 081303 (2008).
- [61] Ji Young Lee, Jun-Hyung Cho, and Zhenyu Zhang, “Quantum size effects in competing charge and spin orderings of dangling bond wires on Si(001),” *Phys. Rev. B* **80**, 155329 (2009).
- [62] R. Robles, M. Kepenekian, S. Monturet, C. Joachim, and N. Lorente, “Energetics and stability of dangling-bond silicon wires on H passivated Si(100),” *J. Phys.: Condens. Matter* **24**, 445004 (2012).
- [63] Mikaël Kepenekian, Frederico D. Novaes, Roberto Robles, Serge Monturet, Hiroyo Kawai, Christian Joachim, and Nicolás Lorente, “Electron transport through dangling-bond silicon wires on H-passivated Si(100),” *J. Phys.: Condens. Matter* **25**, 025503 (2013).
- [64] Mads Engelund, Nick Papior, Pedro Brandimarte, Thomas Frederiksen, Aran Garcia-Lekue, and Daniel Sánchez-Portal, “Search for a metallic dangling-bond wire on n-doped H-passivated semiconductor surfaces,” *J. Phys. Chem. C* **120**, 20303–20309 (2016).
- [65] Miao Zhou, Zheng Liu, Zhengfei Wang, Zhaoqiang Bai, Yuanping Feng, Max G. Lagally, and Feng Liu, “Strain-engineered surface transport in Si(001): Complete isolation of the surface state via tensile strain,” *Phys. Rev. Lett.* **111**, 246801 (2013).
- [66] J. Munguía, G. Bremond, J. M. Bluet, J. M. Hartmann, and M. Mermoux, “Strain dependence of indirect band gap for strained silicon on insulator wafers,” *Appl. Phys. Lett.* **93**, 102101 (2008).
- [67] Soline Richard, Frédéric Aniel, Guy Fishman, and Nicolas Cavassilas, “Energy-band structure in strained silicon: A 20-band k-p and Bir-Pikus Hamiltonian model,” *J. Appl. Phys.* **94**, 1795–1799 (2003).
- [68] Feng Liu, Minghuang Huang, P. P. Rugheimer, D. E. Savage, and M. G. Lagally, “Nanostressors and the nanomechanical response of a thin silicon film on an insulator,” *Phys. Rev. Lett.* **89**, 136101 (2002).
- [69] J. Munguía, J.-M. Bluet, O. Marty, G. Bremond, M. Mermoux, and D. Rouchon, “Temperature dependence of the indirect bandgap in ultrathin strained silicon on insulator layer,” *Appl. Phys. Lett.* **100**, 102107 (2012).
- [70] Kamyar Saeedi, Stephanie Simmons, Jeff Z. Salvail, Phillip Dluhy, Helge Riemann, Nikolai V. Abrosimov, Peter Becker, Hans-Joachim Pohl, John J. L. Morton, and Mike L. W. Thewalt, “Room-temperature quantum bit storage exceeding 39 minutes using ionized donors in silicon-28,” *Science* **342**, 830–833 (2013).
- [71] Jarryd J. Pla, Kuan Y. Tan, Juan P. Dehollain, Wee H. Lim, John J. L. Morton, Floris A. Zwanenburg, David N. Jamieson, Andrew S. Dzurak, and Andrea Morello, “High-fidelity readout and control of a nuclear spin qubit in silicon,” *Nature* **496**, 334–338 (2013).
- [72] J. Salfi, J. A. Mol, R. Rahman, G. Klimeck, M. Y. Simmons, L. C. L. Hollenberg, and S. Rogge, “Quantum simulation of the Hubbard model with dopant atoms in silicon,” *Nat. Commun.* **7**, 11342 (2016).
- [73] M. H. Mohammady, G. W. Morley, A. Nazir, and T. S. Monteiro, “Analysis of quantum coherence in bismuth-doped silicon: A system of strongly coupled spin qubits,”

- Phys. Rev. B **85**, 094404 (2012).
- [74] Gary Wolfowicz, Alexei M. Tyryshkin, Richard E. George, Helge Riemann, Nikolai V. Abrosimov, Peter Becker, Hans-Joachim Pohl, Mike L. W. Thewalt, Stephen A. Lyon, and John J. L. Morton, “Atomic clock transitions in silicon-based spin qubits,” *Nat. Nano.* **8**, 561–564 (2013).
- [75] Roberto Lo Nardo, Gary Wolfowicz, Stephanie Simmons, Alexei M. Tyryshkin, Helge Riemann, Nikolai V. Abrosimov, Peter Becker, Hans-Joachim Pohl, Michael Steger, Stephen A. Lyon, Mike L. W. Thewalt, and John J. L. Morton, “Spin relaxation and donor-acceptor recombination of Se^+ in 28-silicon,” *Phys. Rev. B* **92**, 165201 (2015).
- [76] Kevin J. Morse, Rohan J. S. Abraham, Helge Riemann, Nikolai V. Abrosimov, Peter Becker, Hans-Joachim Pohl, Michael L. W. Thewalt, and Stephanie Simmons, “A photonic platform for donor spin qubits in silicon,” (2016), arXiv:1606.03488 [cond-mat, physics:quant-ph].

Optimizing surface defects for atomic-scale electronics: Si dangling bonds

Supplemental material

Peter Scherpelz^{1,*} and Giulia Galli^{1,2}

¹*Institute for Molecular Engineering,*

The University of Chicago, Chicago, IL, USA

²*Materials Science Division, Argonne National Laboratory, Argonne, IL, USA*

(Dated: May 25, 2017)

In this supplemental material we include detailed notes on the calculations which were reported in the main text, as well as convergence studies, and results at the PBE level when only hybrid results were shown in the main text.

NEUTRAL DB STATE CALCULATIONS

Calculation details

Our basic calculations use the generalized gradient approximation functional developed by Perdew, Burke, and Ernzerhof (PBE) [1]. All calculations use Troullier-Martins norm-conserving pseudopotentials [2] generated by D. Ceresoli [3] and a wavefunction energy cutoff of 40 Ry. The vacuum between slabs is 8.9 Å, and a $2 \times 2 \times 1$ unshifted Monkhorst-Pack [4] grid is used to sample the Brillouin zone (unshifted Monkhorst-Pack grids are used throughout this work).

The dielectric-based hybrid calculations used a 40 Ry wavefunction energy cutoff, and an 80 Ry cutoff for the exact exchange (Fock) operator. Only the Γ -point was used to sample the Brillouin zone. Finally, G_0W_0 calculations were based on DFT calculations using the PBE functional. These calculations used a 30 Ry wavefunction energy cutoff, the Γ -point only, and $N_{\text{PDEP}} = 3072$ [5].

For this section the silicon surface was modeled as a symmetric slab, with one DB on each surface. The initial lattice was built using the minimum-energy lattice constant for bulk Si using the PBE functional, which was found to be 5.4653 ± 0.0003 Å. Approximate positions for the monohydride termination were put in by hand, the appropriate hydrogen atoms were removed to create DBs, and atom positions were randomly perturbed to break any artificial symmetries. The full slab was then relaxed until forces on the atoms were less than $0.013 \text{ eV}/\text{Å}$. The crystal used for the hybrid calculation was not separately relaxed. A 6×6 (4×4) horizontal supercell was used for 12 layers and fewer (more than 12 layers). Here we use the notation $x \times y$ to indicate x atoms perpendicular to the dimer rows by y atoms parallel to the dimer rows in a given layer.

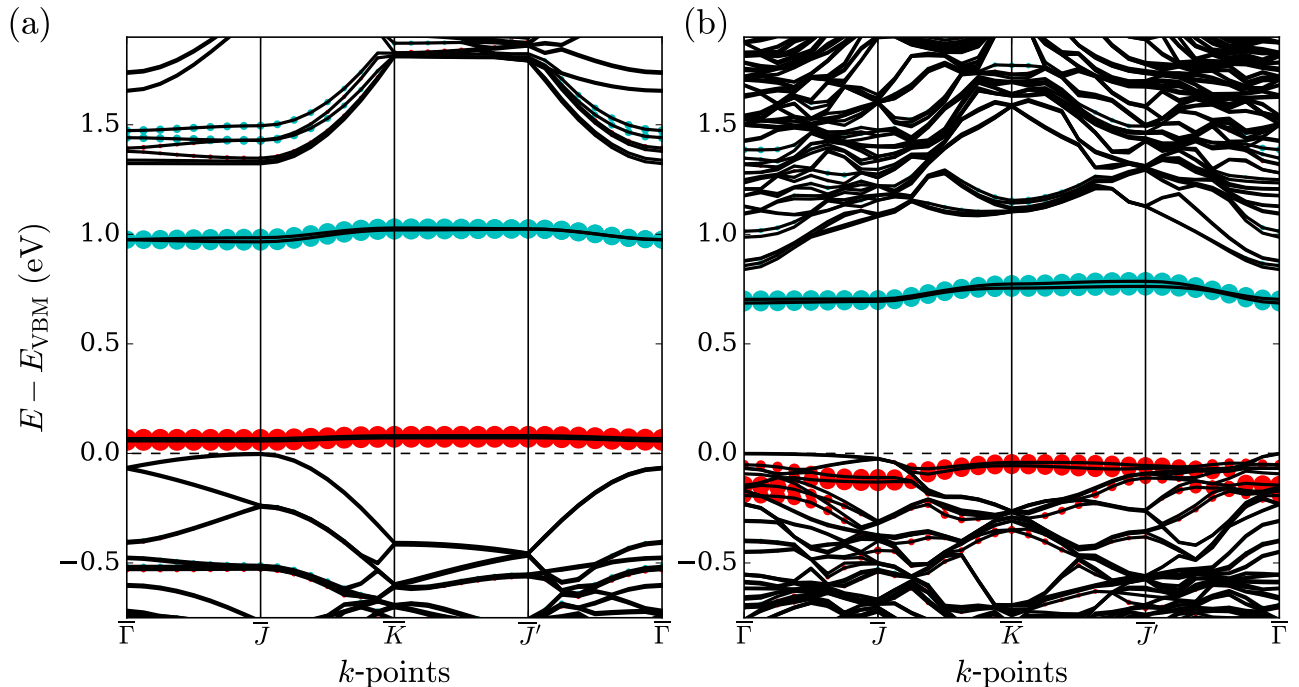


FIG. 1. Band plots corresponding to the (a) 4- and (b) 16-layer calculations shown in Figure 1(a) of the main manuscript. The circles show the proportion of overlap that a given Kohn-Sham eigenstate has with the atomic wavefunctions of the Si atoms with DBs; the circle area is proportional to the overlap, and red (cyan) colors correspond to the overlap for spin-up (spin-down) eigenstates.

Identification of DB states

Dangling bond states were identified by projecting the Kohn-Sham eigenstate wavefunction onto the orthogonalized wavefunctions of the Si atoms with DB states. Isolated DBs had overlaps $|\Psi|^2$ from 0.3 to 0.45. We chose a lower bound of 0.1 to identify a state as having some DB characteristics. While the exact threshold is arbitrary, in cases where this threshold identified multiple states with DB characteristics, rather than a single isolated DB state, it was visually clear that both states had some degree of mixing with bulk states, as in Figure 1(d) of the main manuscript.

In Figure 1(c) and 1(d) of the main manuscript, the isosurface identifies the surface at which $|\Psi|^2 = 0.0013/\text{\AA}$ for the selected, occupied Kohn-Sham eigenstate, using DBs from the 8- and 16-layer results shown in Figure 1(a).

As an alternate way of visualizing DB character, Figure S1 shows the degree to which each band exhibits overlap with the atomic wavefunctions of the Si atoms with DBs. The

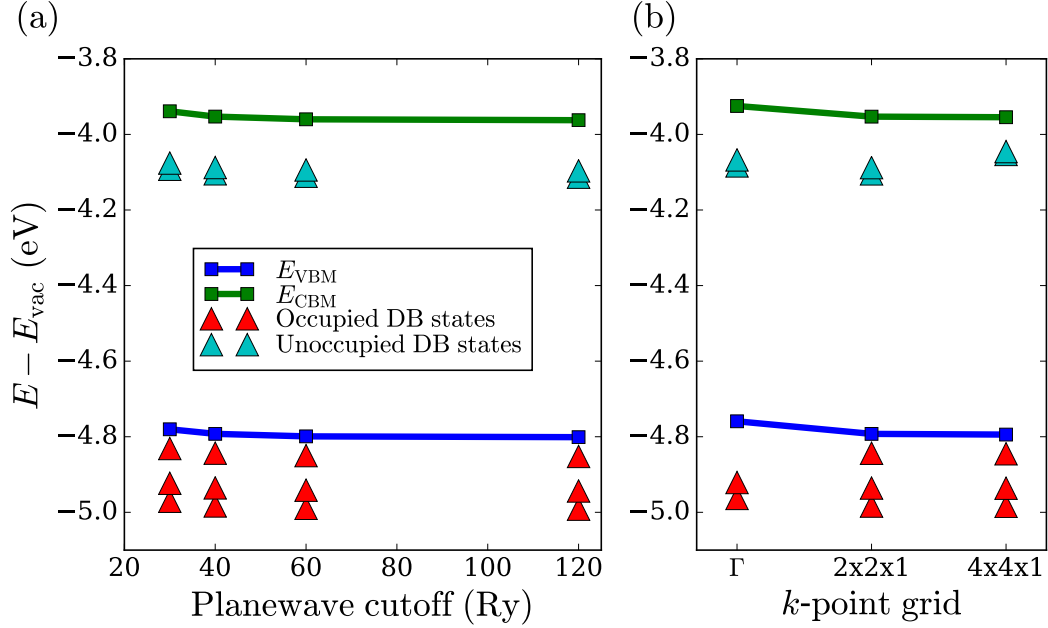


FIG. 2. Convergence of the dangling bond and band positions with regard to the vacuum energy, for 16-layer, 4×4 horizontal unit cell calculations, with symmetric DBs on both surfaces, as in Figure 1 of the main text. (a) Variation of the VBM, CBM, and DB energy levels with energy cutoff of the wavefunction. (b) Convergence with regard to the unshifted k -point mesh used. Note the “missing” occupied DB just below the VBM for the Γ -point-only sampling is a result of a slightly lower overlap with atomic wavefunctions: The state has an overlap with atomic wavefunctions of 0.09, which puts it just below the 0.1 threshold used to plot DB states throughout this work. That state has $E = -4.82$ eV, very close to the $E = -4.84$ eV value for the $4 \times 4 \times 1$ mesh.

4-layer plot clearly exhibits isolated DB states, while the 16-layer plot shows mixing of bulk and DB states, especially near the Γ -point.

Convergence studies

Figure S2 shows the convergence with regard to the plane-wave energy cutoff for the wavefunctions, and the convergence with regard to the k -point mesh used. Overall, compared to 120 Ry, 30 Ry (40 Ry) calculations show deviations of 0.025 eV (0.010 eV). For k -points, Γ -point-only shows deviations up to 0.035 eV, whereas $2 \times 2 \times 1$ values are within 0.002 eV, except for the unoccupied DB states, which seem to be more sensitive and differ by 0.05 eV.

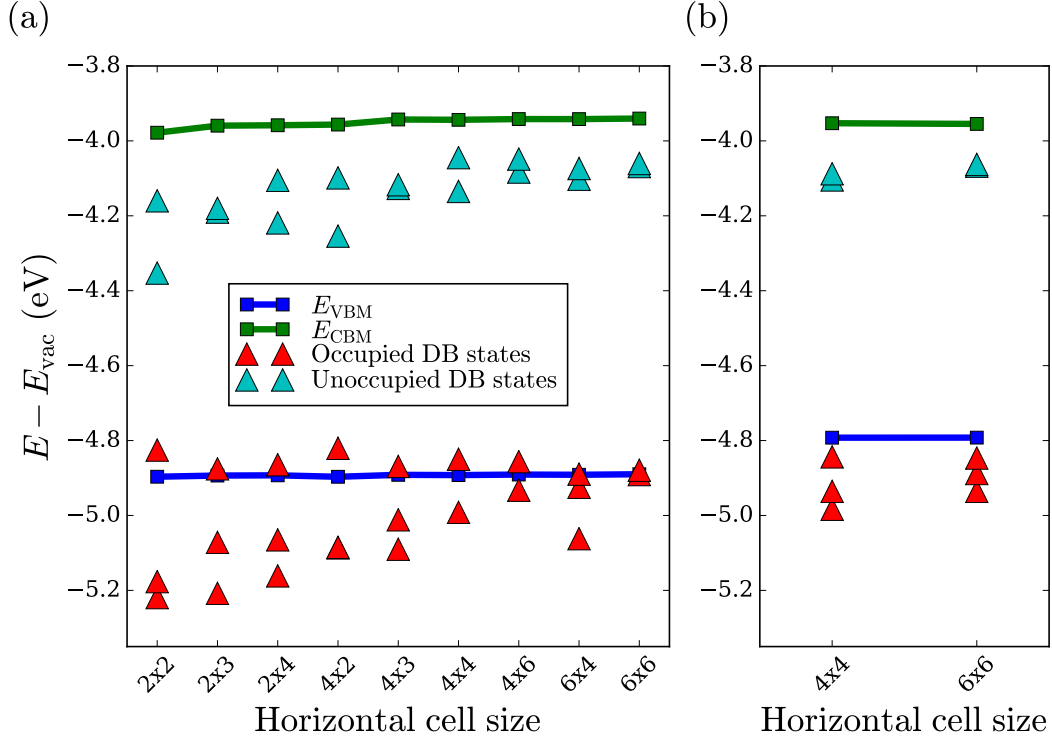


FIG. 3. Convergence of the dangling bond and band positions with regard to the vacuum energy, for symmetric DBs on both surfaces and other parameters as in Figure 1 of the main text. (a) Variation of the VBM, CBM, and DB energy levels for a 12-layer system (b) The same variation for two 16-layer systems.

Figure S3 shows convergence with regard to the horizontal supercell chosen. In all cases, a 4×4 supercell puts the VBM and CBM within 0.004 eV of the 6×6 supercell result. In general, the horizontal geometry primarily affects the degree of dispersion present in the DB states. In the 12-layer case shown in Figure S3(a), dispersion significantly affects DB positions near the VBM for supercells smaller than 6×6 ; in contrast, in Figure S3(b), DB positions are within 0.05 eV between 4×4 and 6×6 systems as the DB positions are no longer close to the VBM.

Other convergence parameters tested, but not plotted due to the minimal changes, are vacuum distance and the convergence threshold for crystal relaxation. For vacuum, we tested the 8.9 Å vacuum distance used in the paper against 17.8 Å; the VBM, CBM, and DB positions relative to vacuum all changed by 0.003 eV or less. For relaxation, we tested the 0.013 eV/Å used in this work against a threshold of 0.003 eV/Å, finding changes of 0.005 eV

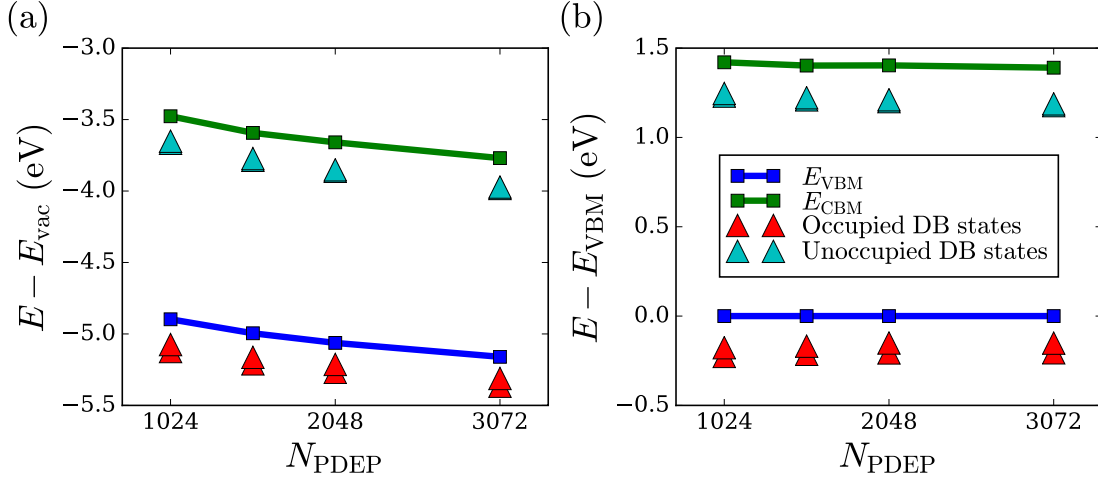


FIG. 4. Convergence of the dangling bond and band positions for varying N_{PDEP} , with other parameters as in Figure 1 of the main text. (a) Variation relative to the vacuum energy, showing changes of up to 0.12 eV between $N_{\text{PDEP}} = 2048$ and $N_{\text{PDEP}} = 3072$. (b) Variation relative to the VBM energy, showing that the relative energy positions of all these states converge very quickly, with differences of 0.02 eV or less between $N_{\text{PDEP}} = 2048$ and $N_{\text{PDEP}} = 3072$.

or less in the VBM, CBM, and DB positions relative to vacuum.

For the G_0W_0 calculation, convergence of N_{PDEP} (see Ref. [5] for details of this parameter) is shown in Figure S4.

CHARGE TRANSITION LEVELS

For charge transition level calculations, a slab with bulk termination on one side, and a monohydride reconstruction with a single DB on the other side, was used. To create the bulk termination we started with a 34-layer slab, using a 2×1 horizontal supercell with a $4 \times 8 \times 1$ k -point mesh. This slab had all Si atoms in their bulk crystal positions. A dihydride hydrogen termination was then put in by hand, and relaxed to $0.013 \text{ eV}/\text{\AA}$ with all Si atoms fixed.

Here one side of the slab was created with the bulk termination used above, and the remaining atoms were then separately relaxed for each charge state and layer number. In these relaxations, the hydrogen positions of the bulk termination were fixed, as were the bottom one, two, or three Si layers (for calculations of 4, 8, and 12 or more total Si layers,

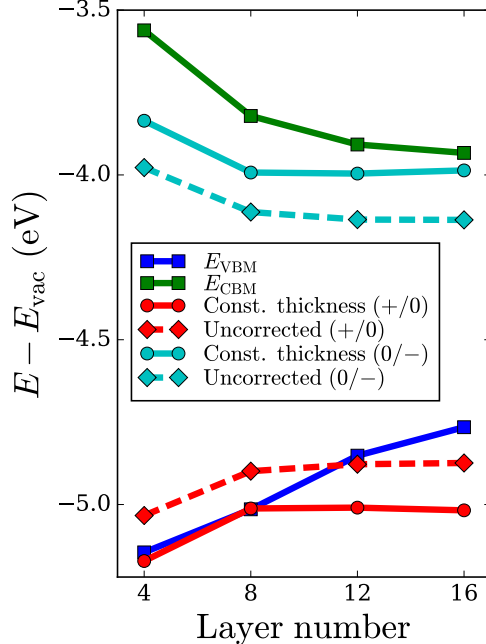


FIG. 5. Adiabatic charge transition levels calculated at the PBE level, otherwise matching the plot in Figure 2 of the main manuscript.

respectively); relaxation was performed for a 4×4 horizontal supercell with a $2 \times 2 \times 1$ k -point mesh, and a 40 Ry wavefunction cutoff, at the PBE level. For Figure 2 of the main paper, 4×6 horizontal supercells were used with a Γ -point only calculation, as 4×4 supercells were too small to align the electrostatic potentials far from the charged defect. A 30 Ry wavefunction cutoff was used, with a 60 Ry cutoff for the exact exchange calculation. The enlargement from 4×4 to 4×6 horizontal supercells was done by using the dimer positions furthest from the DB for the neutrally charged system for the extra two rows. The vacuum was enlarged to 16 Å for all of these calculations to mitigate the effects from charged surfaces.

The charge transition levels were corrected based on the method from Ref. [6]. We first applied a transverse electric field to the neutral system to determine the dielectric constant as a function of z . A model of this functional dependence was created following the procedure in Ref. [6]. A Gaussian was used for the charge density. The results were not sensitive to the width of this Gaussian, which was chosen as 0.6 Å (0.9 Å for negative charges at 12 and 16 layers, which were more spread out). Results were more sensitive to the z position of the Gaussian charge distribution, so it was determined by minimizing the total absolute

difference between the planar-averaged model and DFT potentials (averaged over the x and y directions). Once this was determined, the potential V was computed by solving the Poisson equation, and the electrostatic energy of the system calculated using $E = \frac{1}{2} \int d\mathbf{r} \rho(\mathbf{r})V(\mathbf{r})$ [6]. Finally, the energy correction was calculated as the difference between this energy for the periodic system, and the energy found by uniformly extrapolating the model system to infinite size [6]. Alignment of the electrostatic potential was performed by finding the difference between the potentials averaged over x and z at $y = y_\rho + L_y/2$, where y_ρ is the position of the charge and L_y the supercell size in this direction. Energies were referenced to the VBM of the neutral DB system, which differed from the VBM of the system without defects by 0.002 eV or less.

Figure S5 shows the charge transition levels calculated at the PBE level, with parameters otherwise identical to that in Figure 2 of the main paper. The (+/0) transition moves down in energy to some degree, but trends are very similar.

For convergence of this calculation, we checked other systems at the PBE level, including a 4×8 horizontal supercell with up to a $4 \times 2 \times 1$ k -point mesh, an 8×8 horizontal supercell for 4- and 8-layer systems, and a 4×8 supercell with 32 \AA of vacuum. While uncorrected charge transition levels varied by up to 0.3 eV, corrected transition levels varied by 0.03 eV to 0.06 eV in most cases, with a maximum variation of 0.10 eV for the 4-layer, 8×8 horizontal supercell.

MULTIPLE DB CALCULATIONS

The calculation of a neutral DB pair and DB wire used the same bulk-like dihydride termination for the bottom of the slab as in the previous section, and the PBE functional. To assess convergence, we evaluated the position of the highest-lying occupied DB at the Γ -point relative to the VBM. For the DB pair, we used a 4×6 supercell, and a $2 \times 2 \times 1$ k -point mesh. These runs were compared to calculations using only the Γ point for k -point sampling, finding 0.03 eV variation in the position of the DB relative to the VBM at Γ . Convergence was also checked with 4×10 and 8×6 supercell geometries, for which a 30 Ry wavefunction cutoff and Γ -only k -point sampling was used. The changes in the DB position due to the choice of geometry were 0.012 eV or less. A calculation using the dielectric-dependent hybrid functional was also performed, again using a 30 Ry wavefunction cutoff

and the Γ -point. Here DB positions varied by 0.06 eV or less.

For the DB wire, a 4×2 supercell was used with a $2 \times 4 \times 1$ k -point mesh. This was compared to a $4 \times 8 \times 1$ k -point mesh, finding 0.003 eV variation in the position of the DB relative to the VBM at Γ . Supercells of 4×4 ($2 \times 2 \times 1$ k -point mesh), 8×2 ($1 \times 4 \times 1$ k -point mesh), and (for the 4-layer system) 8×4 ($1 \times 2 \times 1$ k -point mesh) were performed, showing variation of 0.04 eV or less in the DB position when compared to the base calculation. Finally, calculations using the dielectric-dependent hybrid functional also showed variation of 0.04 eV or less in the DB position relative to the VBM.

The overlap was calculated and displayed as for Fig. S1, except that the coloring was the same for spin-up and spin-down eigenstates.

STRAIN CALCULATIONS

For strained systems in the main manuscript, all calculations including relaxations were performed with the HSE hybrid functional. Bulk calculations were used to determine the minimum-energy lattice constant for HSE as 5.4364 ± 0.0003 Å. Biaxial strain was then applied to bulk crystals, and the z -direction lattice constant that produced a minimum energy was found. For each strain value, the appropriate z -direction lattice constant was found to an accuracy of between ± 0.0008 Å (for 0.5% strain) and ± 0.005 Å (for 3% strain).

Figure 4(a) in the manuscript used a slab that was bulk-terminated on both sides. This bulk termination was created by relaxing hydrogen atoms on an 18-layer, fixed Si slab for each strain value. Layers were then added or subtracted from the Si slab to generate 10-, 14-, and 34-layer slabs; no relaxation of Si atoms was performed. In these calculations, a 2×1 horizontal supercell was used with a $4 \times 8 \times 1$ k -point mesh. A 40 Ry wavefunction cutoff was used with an 80 Ry cutoff for the exact exchange calculation.

Figure 4(b) of the manuscript used a 4×4 horizontal supercell with Γ -point only sampling [7]. One surface had the typical monohydride reconstruction with a single DB; bulk termination was used on the other side. Parameters, including lattice constants and hydrogen positions for the bulk termination, otherwise matched those in Figure 4(a). A relaxation of the crystal was performed using the HSE hybrid functional, with the bottom H and Si layers fixed as for the bulk termination in Figure 2.

PBE calculations were also performed for the calculations in Figure 4(a), starting with

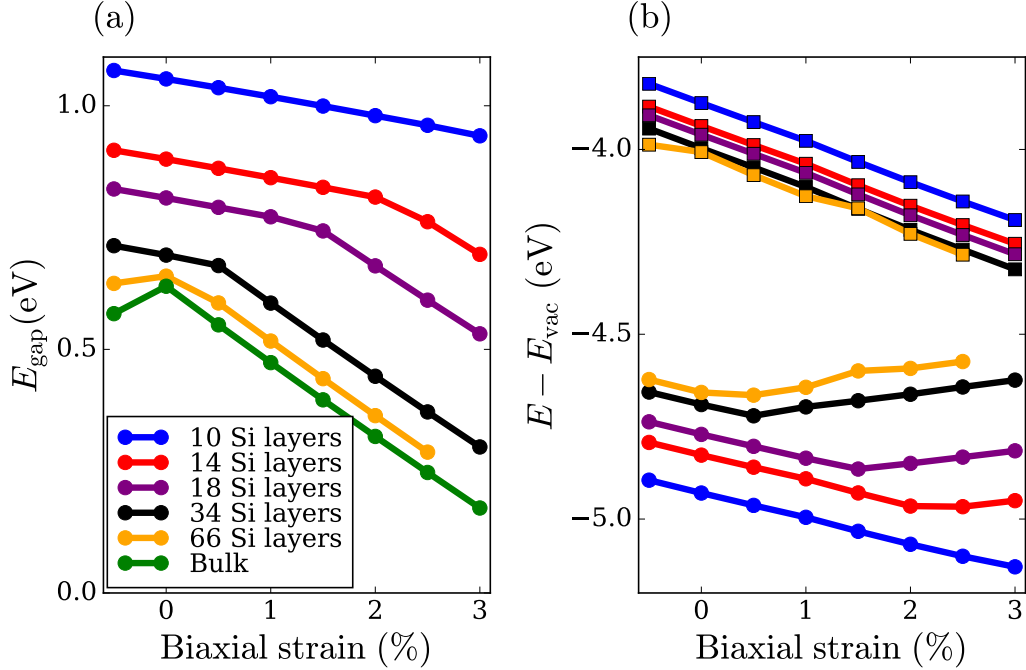


FIG. 6. Variation of energy levels with strain, based on PBE-level calculations; other parameters match those of Figure 4 of the manuscript. (a) Variation of the band gap vs. strain. (b) Variation of the VBM (circles) and CBM (squares) positions vs. strain.

the minimum-energy lattice constant for PBE, and using the bulk-termination hydrogen positions calculated for Figure 2 of the manuscript. These results are shown in Figure S6. The minimum VBM positions relative to vacuum are the same as for the HSE results.

For these thin slabs, the choice of termination does seem to have an effect on the biaxial strain at which the minimum VBM energy is found. This is shown for slabs created with monohydride termination on both sides at the PBE level in Figure S7. The atomic positions were relaxed with no atoms fixed in this case. While the minimum VBM energy moves to lower strain values, the qualitative behavior is similar. The most physically relevant case for a silicon-on-insulator system is likely that of one monohydride surface, i.e. that in Figure 4(b) of the main manuscript, which shows a VBM minimum at 2.5% tensile strain for a 10-layer slab.

* pscherpelz@uchicago.edu

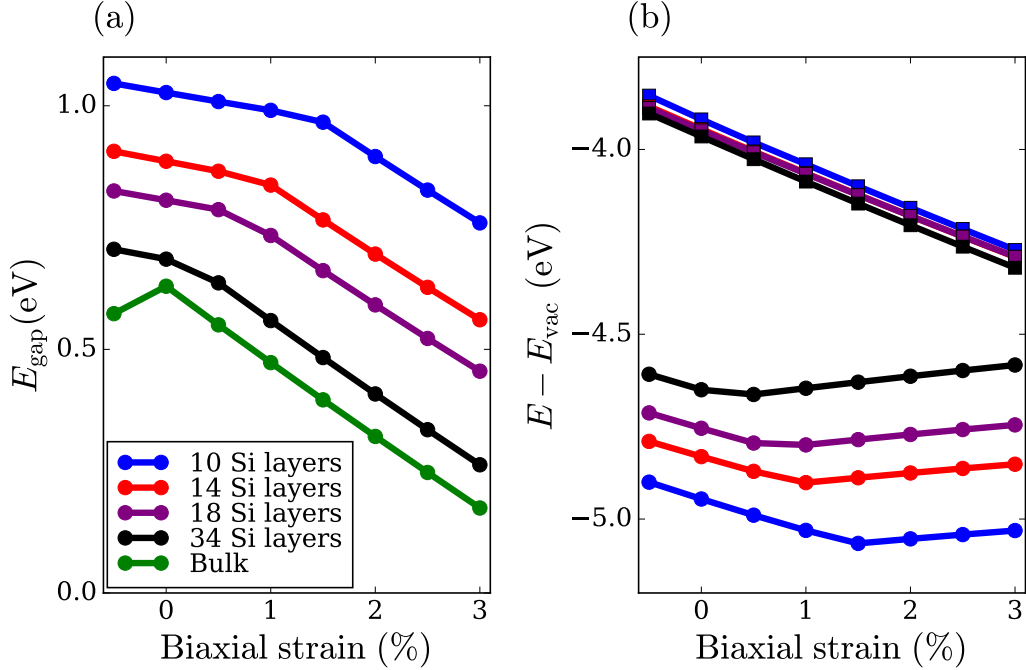


FIG. 7. Variation of energy levels with strain, based on PBE-level calculations, for slabs terminated with monohydride reconstructions and fully relaxed. (a) Variation of the band gap vs. strain. (b) Variation of the VBM (circles) and CBM (squares) positions vs. strain.

- [1] John P. Perdew, Kieron Burke, and Matthias Ernzerhof, “Generalized gradient approximation made simple,” *Phys. Rev. Lett.* **77**, 3865–3868 (1996).
- [2] N. Troullier and José Luís Martins, “Efficient pseudopotentials for plane-wave calculations,” *Phys. Rev. B* **43**, 1993–2006 (1991).
- [3] Davide Ceresoli, “Pseudopotentials,” <https://sites.google.com/site/dceresoli/pseudopotentials>, (accessed May 20, 2016).
- [4] Hendrik J. Monkhorst and James D. Pack, “Special points for brillouin-zone integrations,” *Phys. Rev. B* **13**, 5188–5192 (1976).
- [5] Marco Govoni and Giulia Galli, “Large scale GW calculations,” *J. Chem. Theory Comput.* **11**, 2680–2696 (2015).
- [6] Hannu-Pekka Komsa and Alfredo Pasquarello, “Finite-size supercell correction for charged defects at surfaces and interfaces,” *Phys. Rev. Lett.* **110**, 095505 (2013).
- [7] For biaxial strains of 1.5%, 2.0%, and 2.5%, technical convergence problems led us to use a $2 \times 2 \times 1$ k -point mesh, but with only a single \mathbf{q} vector, $\mathbf{q} = 0$.